

Imprint-Templated Nanocoax Array Architecture: Fabrication and Utilization

**B. Rizal, F. Ye, P. Dhakal, T.C. Chiles, S. Shepard, G. McMahon, M.J. Burns,
and Michael J. Naughton**

18.1 Introduction

Arrays of vertically-oriented cylindrical, coaxial and triaxial nanostructures are fabricated from polymer nanopillar arrays prepared by nanoimprint lithography. With particular process modifications, these arrays have wide potential utility, including as molecular-scale biological (biomarker, pathogen, etc.) and chemical (explosives, environmental agents, etc.) sensors, high density neuroelectronic interfaces and retinal prostheses, radial junction photovoltaic solar cells, ultracapacitors, and optical metastructures. We report on their fabrication and example utilizations in the latter of these areas, with arrays of typical area density 10^6 mm^{-2} .

Vertically-oriented metallic nanowire and semiconducting or insulating nanopillar arrays are finding increasing use for a wide range of novel and enabling applications in, for example, electronics [1], photovoltaics [2, 3], optics [4, 5], and biochemical sensing [6–9]. Metal nanowire arrays are usually formed by electrodepositing metal in the pores of a nanoporous template, such as anodized aluminum oxide (AAO) or polycarbonate track-etch membranes, and removing/dissolving the template. Semiconducting nanowire arrays can be formed by etching a crystalline semiconductor such as silicon, or by epitaxially growing wires on a crystalline substrate. AAO-based nanowire arrays are quasi-ordered in the plane, while semiconductor nanopillar arrays can be random or well-ordered.

B. Rizal • F. Ye • P. Dhakal • M.J. Burns • M.J. Naughton (✉)
Department of Physics, Boston College, Chestnut Hill, MA 02467, USA
e-mail: naughton@bc.edu

T.C. Chiles
Department of Biology, Boston College, Chestnut Hill, MA 02467, USA

S. Shepard • G. McMahon
Nanofabrication Clean Room, Boston College, Chestnut Hill, MA 02467, USA

Nanoimprint lithography (NIL) is a useful technique for rapid and inexpensive replication of nanostructures [10], including those with 3D features such as the nanowire/pillar arrays of interest here. NIL involves coating a prepared “master” nanostructure with an elastomer to form a mold that serves as the negative of the master. A common elastomer is polydimethyl-siloxane (PDMS). After separation from the master, this mold is used to stamp imprint its shape onto a another resist atop a substrate [11], forming a nearly exact replica of the master. Due to the properties of the stamp, even nontrivial 3D structures can be accurately replicated with NIL. Aside from its nanoscale fidelity, perhaps the greatest advantage of the NIL technique is its ability to produce a large number of replicas from a single master.

One structure in which these virtues are manifest is a nanocoaxial array. That is, NIN-prepared nanopillar arrays can be used as starting points for the fabrication of vertically-oriented mono-axial (solid or hollow cylinders), coaxial, triaxial, *etc.* arrays, which have a number of potential technological uses. Here, we describe the NIL-initiated fabrication of variants of such arrays, and their potential utilization as optical waveguides and metamedia.

18.2 Fabrication

18.2.1 Nil Replication of Nanopillar Arrays

As mentioned, NIL utilizes an elastomer to make a flexible mold from a robust master and a photopolymer, such as a photoresist (PR), to make polymeric replicas of the master. As NIL masters in this report, silicon nanopillar (Si-NP) arrays were prepared by a combination of thermal oxidation and reactive ion etching of silicon substrates that were photolithographically patterned. Typical Si-NP dimensions were 2 μm height and 200 nm diameter, in hexagonal close-packed arrays with periodicity/pitch between 0.8 and 1.5 μm , on substrates containing $10 \times 20 \text{ mm}^2$ areas of Si-NP arrays. In addition to vertical pillars, conical and sloped cross-section pillars were prepared with similar average dimensions. These latter ones can facilitate improved step coverage (conformality) of subsequent coatings, relative to that achievable with strictly vertical pillars. PDMS molds were prepared by NIL using a custom clamp apparatus that also facilitated subsequent thermal and/or photopolymerization of resist for replicas. We used SU-8 [12] resist for the NP replicas, chosen for its relatively low glass transition temperature, low volume shrinkage coefficient, and wide range of operating temperatures. Application of heat and pressure between the mold and the substrate coated with SU-8 helps to transfer the pattern from mold to substrate. A single mold can be used to make many replicas without requiring cleaning, and many replicas can be made from a single master. Figure 18.1 shows scanning electron microscope (SEM) images of a representative Si-NP master/PDMS stamp/SU-8 replica set. Note the high fidelity of the replicant

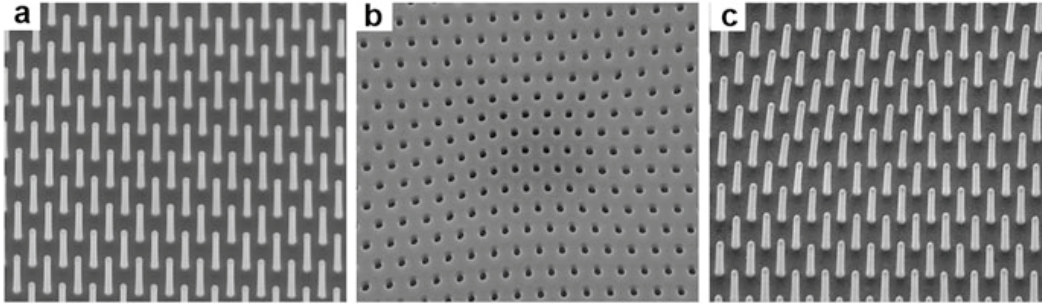


Fig. 18.1 SEM images of the SUV-NIL process. (a) Arrays of vertical 2 μm -tall Si nanopillars of period 1.5 μm used as master. (b) PDMS mold of the master. (c) SU-8 replica of the master

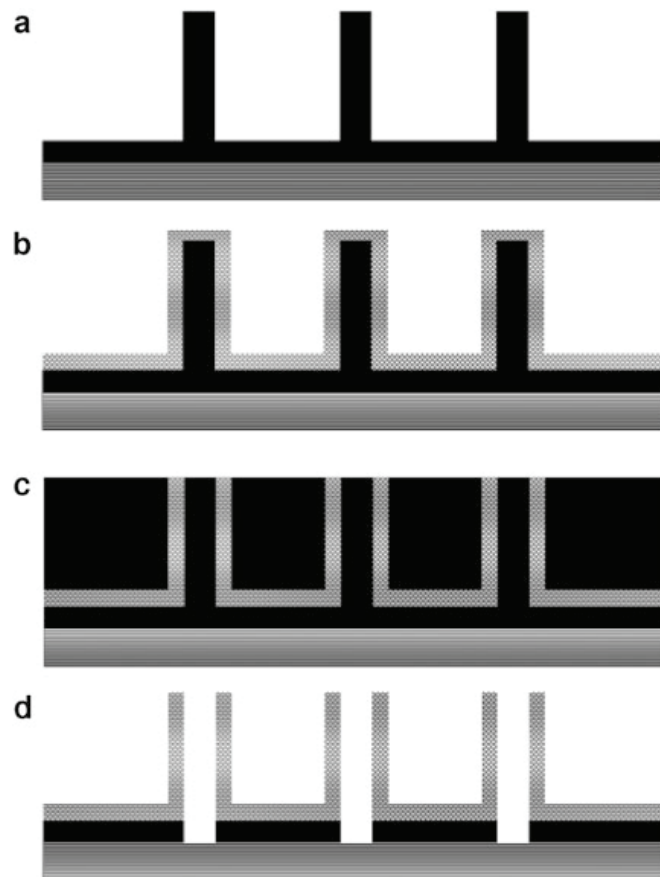
features with respect to the master. Below, we describe the fabrication and potential applications of vertically-oriented arrays of metallic nano-cylinder, coax, and triax arrays of SU-8 nanopillars made by the NIL process.

18.2.2 *Fabrication of Hollow Metal Nanocylinders*

The simplest nanopillar array-based structure to fabricate via NIL, aside from nanopillar replicas themselves, is a metal cylinder. To make this structure, we metallized the surfaces of SU-8 nanopillar arrays using a PVD system (usually sputter deposition, though thermal and electron beam evaporation can be employed, albeit with reduced conformality) followed by mechanical polishing to remove metal from the top of the nanopillar, and reactive ion etching (RIE) to remove the polymer from the core of the pillar. To avoid SU-8 nanopillar shape degradation due to plastic flow, this metallization needs, as do all subsequent process steps, to be performed at the lower of the glass transition or polymerization temperature of SU-8. Figure 18.2 shows an illustration of the fabrication scheme for nanocylinder arrays. We used 20–100 nm thick Au, Ag, Cr, Ti and combinations thereof for the metallization step, deposited by sputter deposition, as well as Pt by atomic layer deposition (ALD). The thickness of the sputtered metal coating in vertical nanostructures was not always uniform, being typically 10–20% thicker (measured radially) at the top than at the bottom. Not surprisingly, we found improved conformality of coating on conical, compared to strictly vertical structures.

Typically, and depending on pillar height, the radial thickness of the metal on the wall of the conical pillar was one third to one half that of the vertical thickness of the metal on the “floor” between pillars. Before polishing, support for each nanopillar was provided by coating the array with a second SU-8 stabilizing layer, filling the space between the pillars to a thickness comparable to or greater than the height of the pillars. Mechanical polishing is then done by using suspensions of 50 nm alumina nanoparticles on a vibratory polisher, typically for several hours per run. Polishing/inspection cycles continue until the metal on the top of the pillars

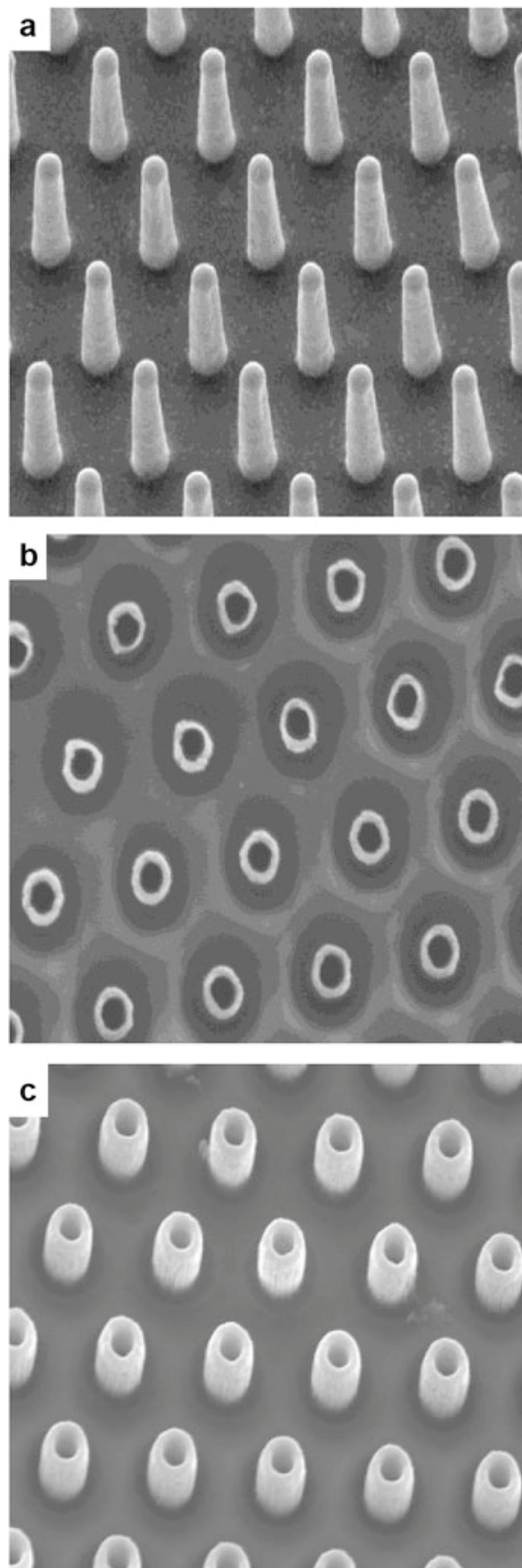
Fig. 18.2 Summary of the procedure used to fabricate arrays of hollow metallic nanocylinder from the polymer pillars. **(a)** Polymer nanopillar array. **(b)** Inner metal coating. **(c)** Polymer coating; **(d)** Etching of polymer



has been either exposed or fully removed, thus exposing the SU-8 centers. RIE is performed in a Plasma-Therm Versaline inductively-coupled reactive ion etch (ICP-RIE) system with 20 SCCM flow of CF_4 at 0.5 Pa pressure, 200 W power and 355 V self-bias conditions, which produces an etch rate ~ 5 nm/s for SU-8. Figure 18.3 shows SEM images at different stages of fabrication of arrays of hollow metallic (Au) nanocylinders of 1.3 μm pitch, 300 nm inner diameter, 450 nm outer diameter and 1.8 μm height. We have made similar arrays with pitches between 800 nm and 1.5 μm . In addition, inner diameter tuning is facilitated by isotropic or anisotropic etching of the master Si-NP arrays or of the replicated SU-8 arrays, outer diameter by metal film deposition time, height by polishing time, and depth (inside the metal cylinder) by etch time and/or process (*i.e.* wet or dry etch).

As such, this fabrication method has been used to make arrays of different metals, pitch, radius, and height of hollow metallic nanocylinders. The pitch of the arrays always matches that of the master used to make the replica. Our template method may be an improvement over a previously reported method [13], especially to make arrays of nanocylinders of hard metals like Cr and W without artifacts and defects. Figure 18.4 shows two examples with Cr.

Fig. 18.3 SEM images of a hollow gold cylinder array at different stages of fabrication. **(a)** Metallized SU-8 nanopillar array of pitch $1.3\ \mu\text{m}$. **(b)** Polished nanopillar array embedded in SU-8 film. **(c)** Hollow metallic nanocylinder array with $300\ \text{nm}$ inner radii and $1.8\ \mu\text{m}$ height



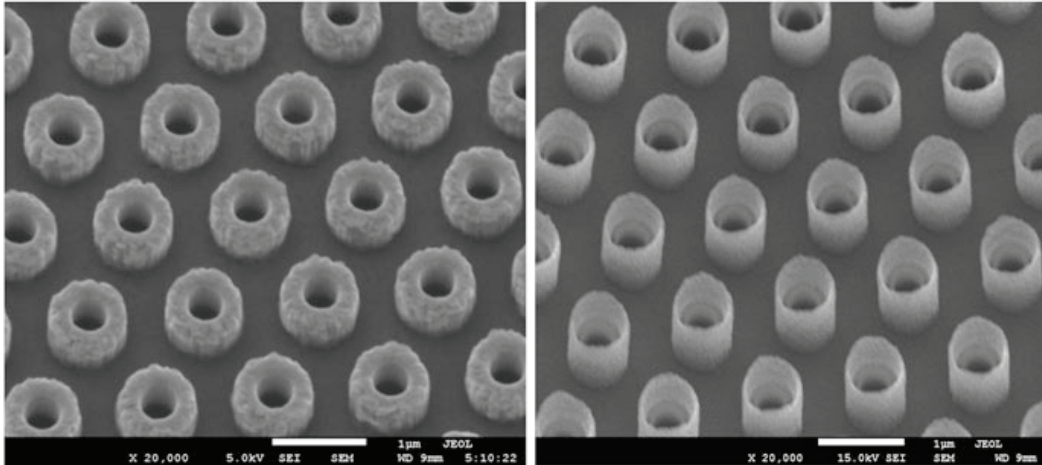


Fig. 18.4 Hollow metallic (Cr) cylinder arrays of various dimensions. Scale bars = 1 μm

18.2.3 Fabrication of Nanocoaxes

To form nanocoaxes, the first steps are as stated above through NP metallization (*i.e.* Figs. 18.2b and 18.3a). Figure 18.5 depicts the steps involved to fabricate arrays picking up from this point. After the initial metallization, we deposit a dielectric layer. We have deposited different kinds of dielectrics using different methods, including ALD, plasma enhanced chemical vapor deposition (PECVD), sputtering, and spin-coating, to deposit films anywhere between 10 and 200 nm thick (measured radially) of porous or nonporous dielectrics such as Al_2O_3 , SiO_2 , Si_3N_4 , polymer, *a*-Si, *etc.* For ALD of Al_2O_3 , we used trimethylaluminum (TMA) as precursor, whereas for PECVD SiO_2 , and Si_3N_4 , a gas mixture with ratio $\text{SiH}_4/\text{N}_2\text{O} : 2/9$ has been used at 200 °C. Reactively-sputtered Al_2O_3 deposition is done by introducing O_2 gas in ratio 1:6 to Ar during deposition of Al at room temperature. Of the three deposition methods, ALD and spin-coating yield the most conformal and dense coatings of dielectrics, especially on strictly vertical structures. In an early nanocoax application, the dielectric annulus was prepared as a radial *p-i-n* junction with amorphous silicon (*a*-Si), so that the array functioned as a photovoltaic solar cell [2].

Next, an outer metal film is deposited, of typical thickness 20–100 nm to form a nanocoaxial structure. For many applications, such as biological, chemical and neurological sensing, and for the study of nanoscopic effects of light propagation, the top ends of coax structures are removed (“decapitated” by mechanical polishing), forming open-ended nanocoaxes, as depicted in Fig. 18.5. In some cases, the arrays are processed further by etching the annuli and/or the cores inside the inner coax metal, by processes similar to those employed in the fabrication of hollow nanocylinder arrays, Figs. 18.2, 18.3, and 18.4 above. Such examples are shown in Fig. 18.6 (including full process steps) and Fig. 18.7 below.

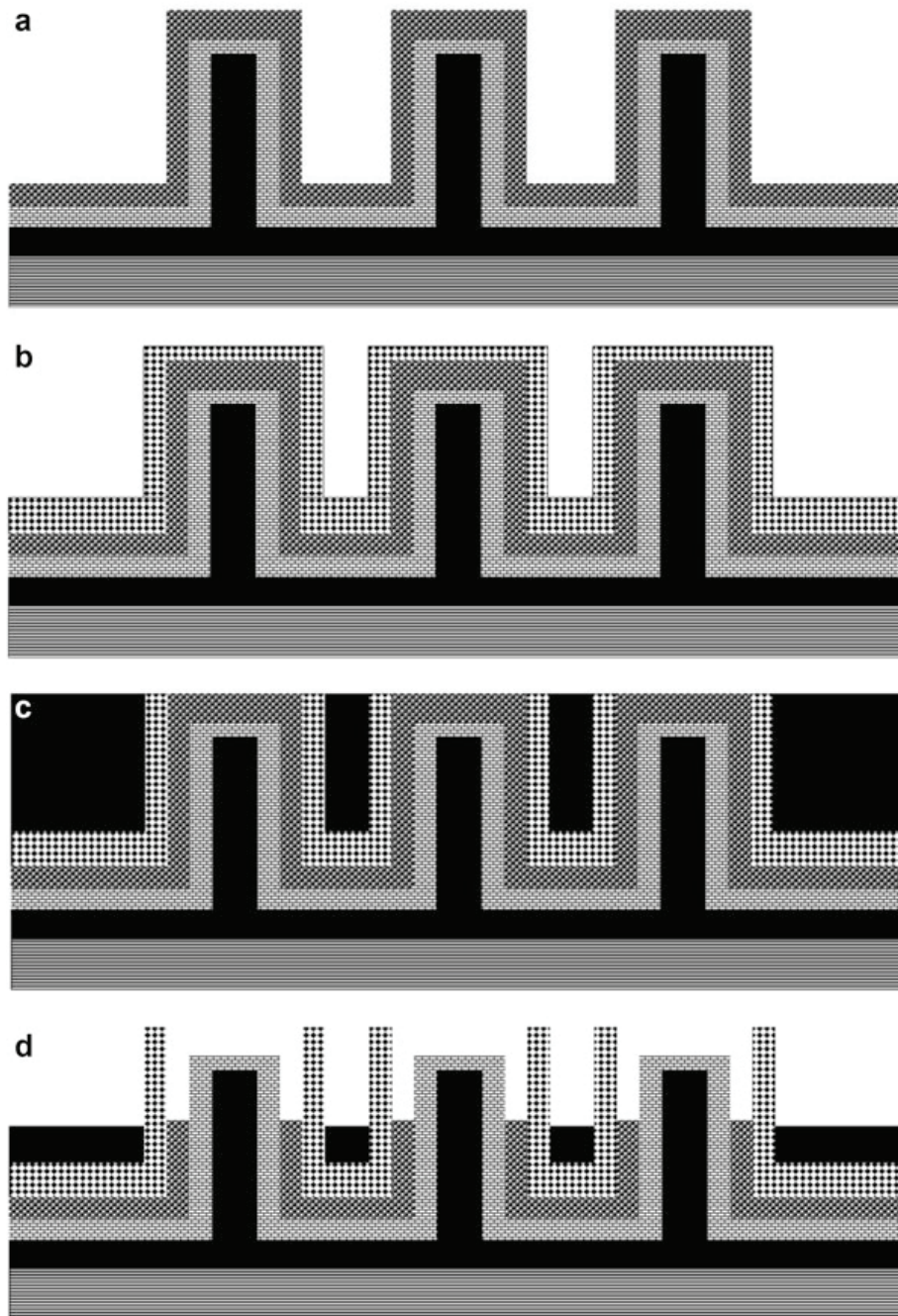


Fig. 18.5 Schematic representations of fabrication process for nanocoax arrays. (a) Dielectric coating. (b) Outer metal coating. (c) Polymer coating. (d) Etching of dielectric

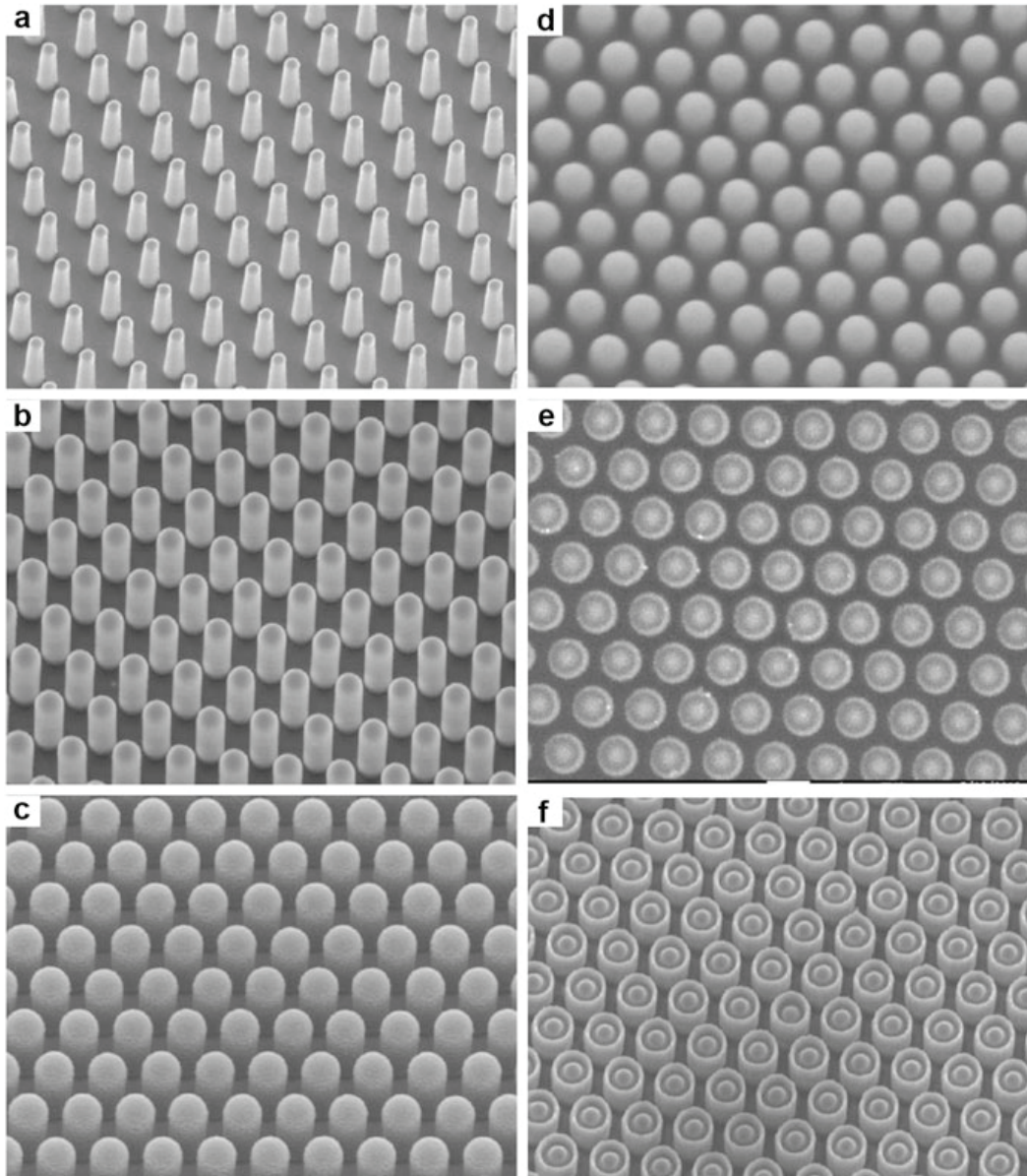


Fig. 18.6 SEM images of the fabrication process for open ended nanocoax structure of $1.3 \mu\text{m}$ pitch and $2 \mu\text{m}$ height. (a) Inner metal coating. (b) Dielectric coating. (c) Outer metal coating. (d) SU-8 coating. (e) Mechanical polishing. (f) Etching of dielectric

18.3 Optical Utilization

18.3.1 *Light Transmission Through Hollow Metallic Nanocylinders*

Hollow metallic nanostructures have interesting optical properties. The top panel of Fig. 18.8 shows the results of finite-difference time-domain (FDTD) simulation of 500 nm light through an array of conical Au nanocylinders of $1.3 \mu\text{m}$ pitch, $1.8 \mu\text{m}$

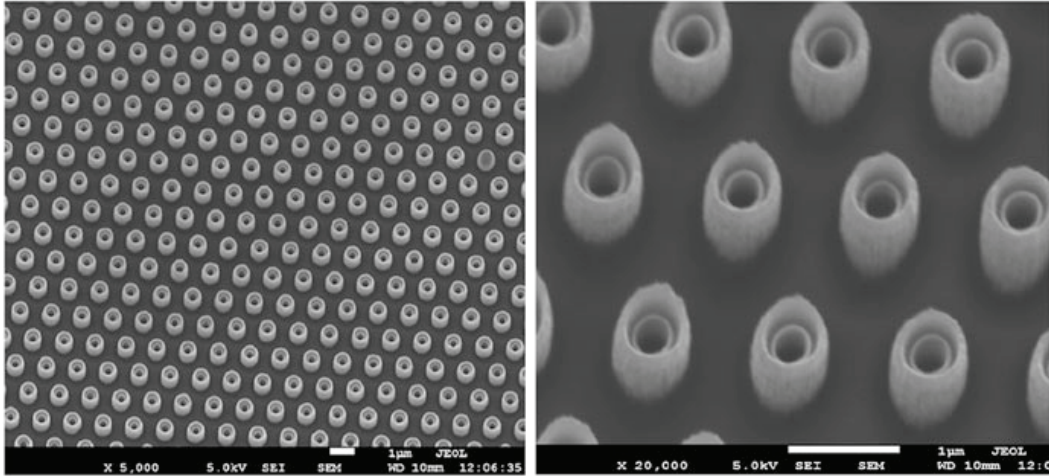


Fig. 18.7 Nanocoax array with hollow core and hollow annulus. Scale bars = 1 μm

height, and 300 nm base diameter. Despite the nanocylinders dimensions being subwavelength in diameter, the simulations indicate that light should be able to propagate through them. This is confirmed in the center panel of Fig. 18.8, in a near-field scanning optical microscope (NSOM/SNOM) image of a sample illuminated from below with $\lambda = 500$ nm light. The bottom panel is an optical micrograph of the sample, illuminated from below with white light, clearly showing light not just emerging from the subwavelength holes, but the mere fact that the microscope formed an image illustrates that the emerging light was able to launch into the far-field. The transmission is dominated by light in the 600–700 nm wavelength range (bright spots are red in color), significantly larger than the inner radius, such that some degree of subwavelength propagation into the far field occurs. This transmission may be associated with resonant coupling of local surface plasmons in the cylindrical cores with incident light [14]. Thus, arrays of such nanocylinders could serve as a basic tool to study and characterize nanoscale manipulation of light.

18.3.2 Light Transmission Through Nanocoaxes

The coaxial cable is known to be an ideal geometry for the efficient propagation of electromagnetic waves, being one of only two configurations (the other being a semi-infinite parallel plate) that propagates a transverse electromagnetic mode (TEM). For perfect electrical conductors, this mode has no cutoff frequency, while the TE_{mn} modes cut off at wavelengths larger than the average of the circumferences of the inner and outer conductors [15]. A nanoscale version of a coax, a nanocoax, operates similarly [16], with the exception that, for high enough frequency (*i.e.* visible), the radiation can interact with the metals comprising the waveguide. Transmission in a nanoscale coax has been shown theoretically to propagate in a

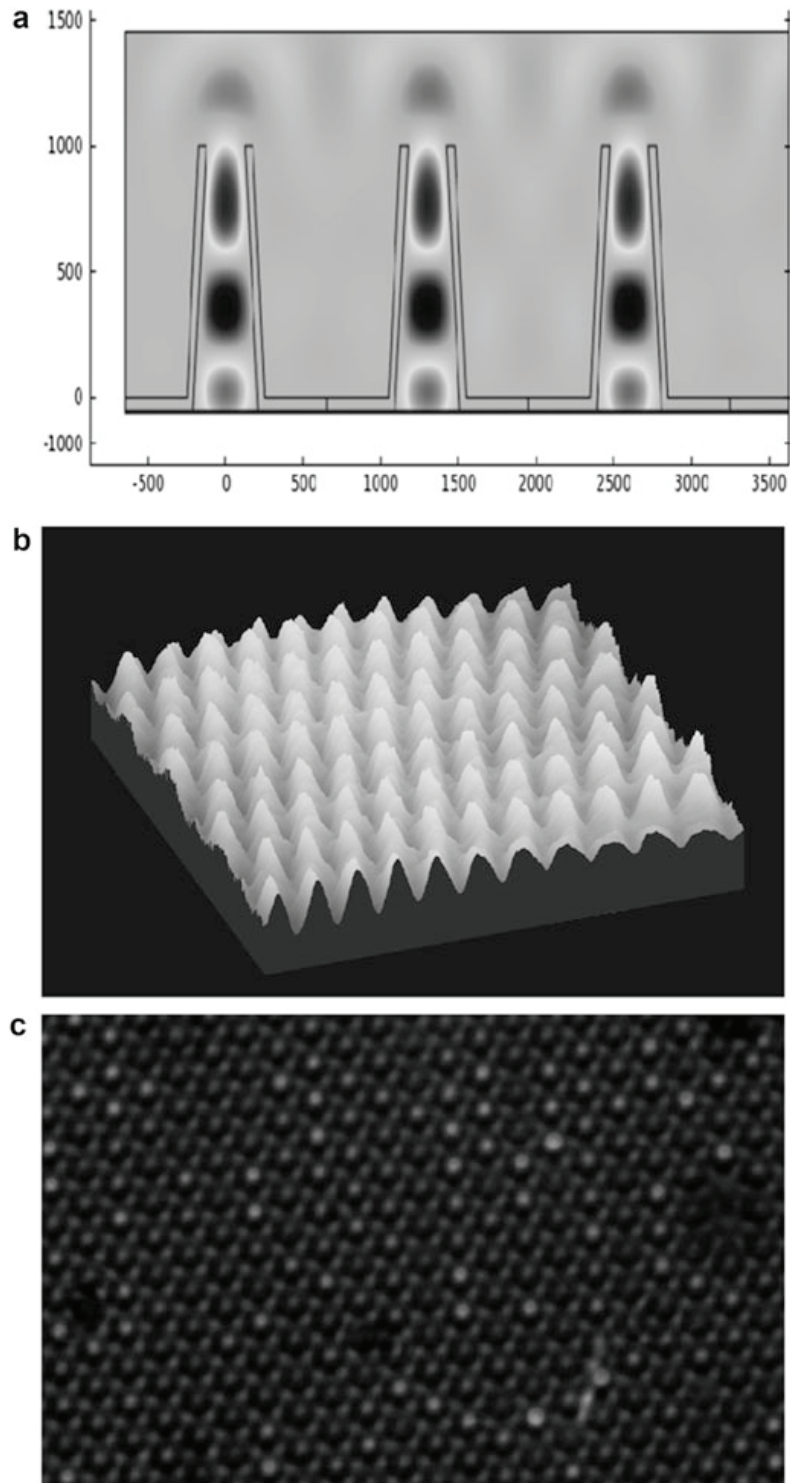


Fig. 18.8 (a) Simulation of light passing through an array of subwavelength nanocylinders as described in the text. (b) NSOM micrograph of 500 nm light passing through an array of subwavelength nanocylinders. (c) Optical micrograph of an array of subwavelength nanocylinders illuminated with light from below, showing transmission peaked in the bright spots

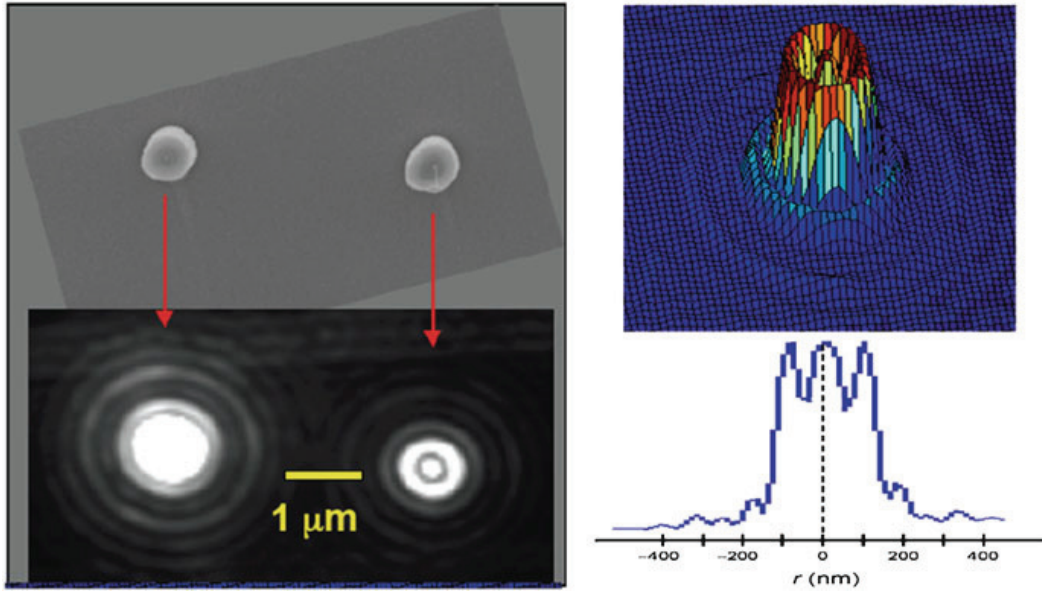


Fig. 18.9 (a) SEM top view of two isolated nanocoaxes with 150 nm diameter core and 100 nm thick annulus. (b) Optical micrograph of light emanating out the tops of the two coaxes, illuminated from below. (c) Light intensity map of right coax. (d) Line cut along a radial direction of transmitted light intensity

TM_{00} mode, which reduces to the TEM in the appropriate wavelength regime [17]. Nanocoaxes fabricated for optical purposes at Boston College indeed have been shown to transmit light for wavelengths larger than the nanocoax [5].

In Fig. 18.9, we show a scanning electron micrograph of two vertically-oriented nanocoaxes surrounded by an optically-opaque (150 nm thick W) film. The dielectric in the annuli of these coaxes is 100 nm thick ALD-deposited Al_2O_3 , and the tops were exposed by focused ion beam milling. Immediately below this SEM is an optical micrograph of the same two nanocoaxes while illuminated by white light from below the opaque film. One can see in the optical image the transmission of the light, including Airy's rings [18] due to the diffraction-limited detection of the optical microscope that is observing the far field radiation emanating from the ends of the nanocoaxes. In the right panels, we show a 3D intensity map of the right nanocoax's emission pattern, and a line cut through the center of that pattern. This latter graph also shows Airy rings as spatial oscillations with a spacing of about 100 nm in the image.

In summary, we used imprint-templated lithography to replicate arrays of silicon nanopillars in SU-8 polymer, and used those replicated arrays to form arrays of metal nanocylinders and nanocoaxes (as well as nanotriaxes, *etc.*, not discussed here). These structures can be employed in a variety of sensing applications, and for the nanoscale manipulation of light, including as radial-junction solar cells and nanophotonic waveguides. Examples of the latter were presented herein.

Acknowledgment This work was supported by the W.M. Keck Foundation and the US National Cancer Institute.

References

1. Duan X, Huang Y, Cui Y, Wang J, Lieber CM (2001) Indium phosphide nanowires as building blocks for nanoscale electronic and optoelectronic devices. *Nature* 409:66–69
2. Naughton MJ, Kempa K, Ren ZF, Gao Y, Rybczynski J, Argenti N, Gao W, Wang Y, Peng Y, Naughton JR, McMahon G, Paudel T, Lan YC, Burns MJ, Shepard A, Clary M, Ballif C, Haug F-J, Söderström T, Cubero O, Eminian C (2010) Efficient nanocoax-based solar cells. *Phys Status Solidi Rapid Res Lett* 4:181–183
3. Paudel T, Rybczynski J, Gao YT, Lan YC, Peng Y, Kempa K, Naughton MJ, Ren ZF (2011) Nanocoax solar cells based on aligned multiwalled carbon nanotube arrays. *Phys Status Solidi A* 208:924–927
4. Sirbuly DJ, Law M, Yan J, Yang P (2005) Semiconductor nanowires for subwavelength photonics integration. *J Phys Chem B* 109:1519–15213
5. Rybczynski J, Kempa K, Herczenski A, Wang Y, Naughton MJ, Ren ZF, Haung ZP, Cai D, Giersig M (2007) Subwavelength waveguide for visible light. *Appl Phys Lett* 90:021104
6. Zhao HZ, Rizal B, McMahon G, Wang H, Dhakal P, Kirkpatrick T, Ren ZF, Chiles TC, Naughton MJ, Cai D (2012) Ultrasensitive chemical detection using nanocoax sensor. *ACS Nano* 6:3171–3178
7. Kabashin AV, Evans P, Pastkovsky S, Hendren W, Wurtz GA, Atkinson R, Pollard R, Podolskiy VA, Zayats AV (2009) Plasmonic nanorod metamaterials for biosensing. *Nat Mater* 8:867–871
8. Holgado M, Barrios CA, Ortega FJ, Sanza FJ, Casquel R, Laguna MF, Banuls MJ, Lopezromero D, Puchades R, Maquaieira A (2010) Label-free biosensing by means of periodic lattices of high aspect ratio SU-8 nanopillars. *Biosens Bioelectron* 25:2553–2558
9. Kubo W, Fujikawa S (2011) Au double nanopillars with nanogap for plasmonic sensor. *Nano Lett* 11:8–15
10. Chou SY, Krauss PR, Renstrom PJ (1996) Imprint lithography with 25-nanometer resolution. *Science* 272:85–87
11. Gates BD, Xu Q, Stewart M, Ryan D, Willson CG, Whitesides GM (2005) New approaches to nanofabrication: molding, printing, and other techniques. *Chem Rev* 105:1171–1196
12. Microchem Corporation, Newton, MA
13. Xu Q, Perez-Castillejos R, Li ZF, Whitesides GM (2006) Fabrication of high-aspect-ratio metallic nanostructures using nanoskiving. *Nano Lett* 6:2163–2165
14. Krishnan A, Thio T, Kim TJ, Lezec HJ, Ebbesen TW, Wolff PA, Pendry J, Martin-Moreno L, Garcia-Vidal FJ (2001) Evanescently coupled resonance in surface plasmon enhanced transmission. *Opt Commun* 200:1–7
15. Pozar D (2012) *Microwave engineering*, 4th edn. Wiley, New York
16. Kempa K, Wang X, Ren ZF, Naughton MJ (2008) Discretely guided electromagnetic effective medium. *Appl Phys Lett* 92:043114
17. Peng Y, Wang X, Kempa K (2008) TEM-like optical mode of a coaxial nanowaveguide. *Opt Express* 16:1758–1763
18. Airy GB (1835) On the diffraction of an object-glass with circular aperture. *Trans Camb Philos Soc* 5:283–291